Perfection of leakage and ferroelectric properties of Ni-doped $BiFeO_3$ thin films

Lingxu Wang[1] ✉, *Shiju Yang*[2], *Fengqing Zhang*[2] ✉, *Suhua Fan*[3]

[1]*School of Civil Engineering and Architecture, University of Jinan, Jinan 250022, Shandong, People's Republic of China*
[2]*School of Materials Science and Engineering, Shandong Jianzhu University, Jinan 250101, Shandong, People's Republic of China*
[3]*Shandong Women's University, Jinan 250300, Shandong, People's Republic of China*
✉ *E-mail: keji424@126.com; zhangfengqing615@163.com*

Published in Micro & Nano Letters; Received on 23rd July 2017; Revised on 21st November 2017; Accepted on 21st December 2017

$BiFe_{1-x}Ni_xO_3$ ($x = 0\%$, 1, 2 and 3%) films were deposited on ITO/glass substrate using sol–gel process. The work reports the impacts of Ni doped on the crystal microstructure, leakage current, conduction mechanism and ferroelectric behaviour systematically. From the XRD analysis, all samples match well with the perovskite structure without impurity phase. Polarisation-electric filed hysteresis loop demonstrates that the optimal Ni-doped content of $BiFeO_3$ films is $x = 2\%$, of which the remnant double polarisation ($2P_r$) is 141.4 μC/cm^2 at the test electric field of 1067 kV/cm. Leakage current density curves show that Ni doping has a great contribution in reducing leakage. The value of leakage is 4.79×10^{-7} A/cm^2 at tested electric field of 300 kV/cm. In addition, the leakage conduction mechanism transforms from the Ohmic conduction under the low electric field into the space charge limited conduction under high electric field. Ni doped does not cause significant change in the conduction mechanism.

1. Introduction: Owing to their particular electrical and optical properties such as ferroelectric, electro-optical effect, ferroelectric thin film materials have a wide variety of applications, including ferroelectric random access memory, non-volatile memory, optical devices [1–4]. Among them, perovskite-type compounds in the traditional ferroelectric film material occupies a large proportion. $BiFeO_3$ (BFO) is a typical perovskite-type structure, with the characteristics of ferroelectricity and ferromagnetic coexistence at room temperature (RT), which shows high Curie temperature ($T_C = 830$°C) and high Neel temperature ($T_N = 370$°C) [1, 5, 6]. In addition, BFO has a large remnant polarisation ($P_r \sim 100$ μC/cm^2) [7–9]. However, BFO films generally have high leakage current density, because of the existence of oxygen vacancies and various oxidation states of Fe ion (Fe^{3+} to Fe^{2+} state), which is the major obstacles to practical application [10, 11]. At present, the performance of BFO film is optimised by improving the preparation process and ion doping [12–14]. From current research results, element doping is proved to be the most effective method. In the experiment, the transition metal Ni, Zn, Mn [15–17] and rare earth metal La, Sm, Y were used to doped in BFO films to improve performance [18–20]. Enhanced ferroelectricity and ferromagnetism, decreased dielectric constant and leakage current have been obtained from Ni-doped BFO films by Liu *et al.* [21]. Kim *et al.* reported that Ho and Ni co-doping could improve the ferroelectric properties and decrease the leakage current density [22]. Singh *et al.* reported that La and Ni co-doping made the leakage current density at 500 kV/cm reduce by approximately three orders of magnitude compared with the pure phase [23].

We know that Ni and Fe are two very similar elements, such as near ionic radius and magnetic. So, in this Letter, we chose Ni^{2+} as doping element to instead of Fe^{3+}. We discussed the structure and properties of the film after substitution. We expected to obtain better ferroelectricity and leakage performance.

2. Experimental: We prepared $BiFe_{1-x}Ni_xO_3$ (BFNO, $x = 0$, 1, 2, 3%) films on the ITO/glass by sol–gel method. The precursor solution was prepared using bismuth nitrate, ferric nitrate and nickel nitrate as solutes and glacial acetic acid, ethylene glycol as solvents. Acetylacetone is added to stabilise the solution. In order to make up for the volatilisation of Bi elements in the annealing process, we increased the content of bismuth nitrate by 5% on the basis of previous exploration. Eventually, the precursor solution concentration is 0.3 mol/L. Precursor solutions first span at a speed of 3500 rpm for 30 s, desiccated at 200°C for 3 min on a hot plate, insulated in the quick anneal oven at 350°C for 180 s, and then annealed in air atmosphere at 500 °C for 300 s. We need to repeat the process 15 times to get the same thickness of the film. In order to test, we need to construct the M-F-M (metal-ferroelectric-metal) capacitor structure. So, we need to sputter Au on the thin film surface using a small ion sputtering instrument.

In this Letter, D8-advance XRD of German Bruker company was used to analyse the properties of the crystalline microstructure of the samples. Multiferroic ferroelectric tester manufactured by Radiant Corporation of USA was used to test the ferroelectric properties.

3. Results and discussions: Fig. 1*a* shows the XRD (θ–2θ) diffraction patterns of BFNO films grown on ITO/glass. It demonstrates that all diffraction peaks of BFNO films match well with the rhombohedral distorted perovskite R3c structure without secondary phase (JCPDS Card No. 86-1518). What is noteworthy is that the relative strength of (012) and (104)/(110) peaks for BFNO films gradually increase as the Ni-doped content increase from 0 to 2%. However, continue to increase the Ni content to 3%, the diffraction peak of (104)/(110) decrease. Which shows that the crystallisation of BFO films become better with the increase of Ni-doped content from 0 to 2%. In the inset of Fig. 1*a*, the grain size (D) of the sample is reckoned according to Scherrer's equation. Result shows that the value of D is 33.1, 34.1, 35.7 and 29.1 nm for the BFNO films with $x = 0$, 1, 2, 3%, respectively. Fig. 1*b* is a magnification of 2θ from 31° to 33°. We can see clearly from the figure that the diffraction peak shifts to a small angle as the Ni-doping concentration increases. This indicates that the Ni ion has replaced the trivalent iron ions and entered the BFO lattice. The reason for this phenomenon may be that the large ion radius of Ni^{2+} (0.069 nm) to replace the smaller ion radius Fe^{3+} (0.0645 nm). The lattice constant of the film increases after doping, and by the Bragg equation $2d \sin\theta = n\lambda$, where λ is constant, the diffraction peak is shifted in the direction of decreasing the diffraction angle (2θ).

The thicknesses of the samples are displayed in Fig. 2. The cross-section SEM image reveals a clear boundary between BFNO/ITO

doi: 10.1049/mnl.2017.0554

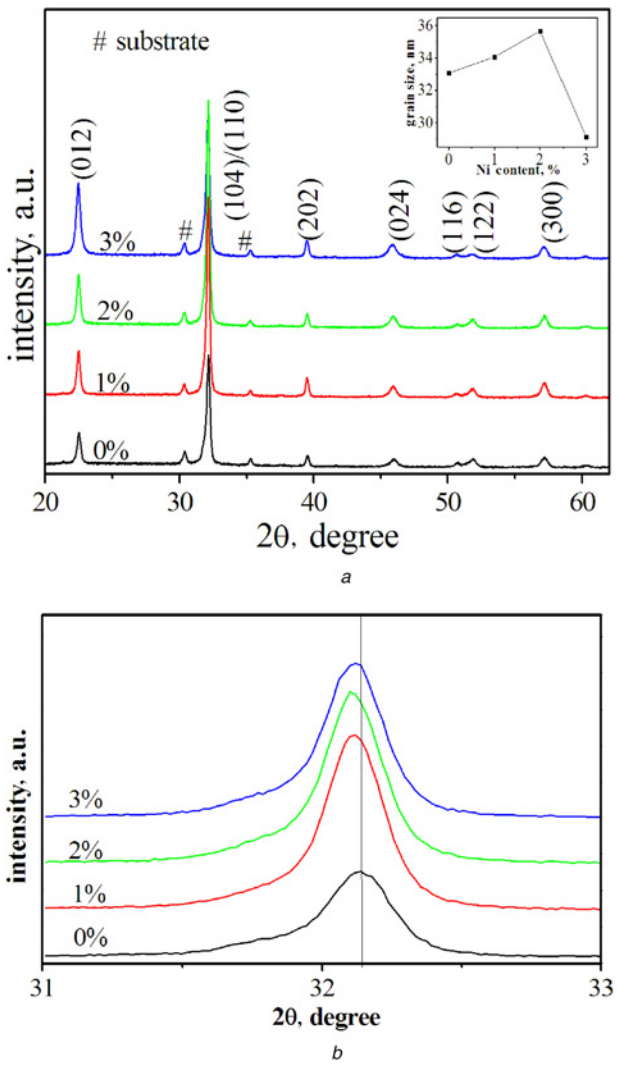

Fig. 1 *XRD diffraction patterns of BFNO films grown on ITO/glass*
a XRD patterns of BFNO thin films. The insets depict the grain size
b XRD patterns in the range of 2θ from 31° to 33°

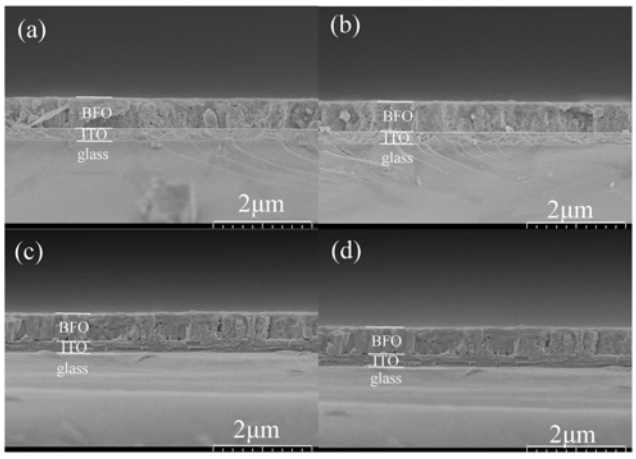

Fig. 2 *Cross-sectional SEM images of BFNO films*
a $x = 0$
b $x = 1\%$
c $x = 2\%$
d $x = 3\%$

and ITO/glass. From up to down are the BFO films, ITO layer and glass layer. From Fig. 2, we can see that the grain growth is good, the thickness is uniformity. In addition, the thickness of films and ITO layer is close to 800 and 200 nm, respectively.

The surface morphological features of the BFNO thin films are shown in Fig. 3. The microstructure of all the four samples is overall densely packed. With the increase of Ni-doping content, the grain size increases first (0–2%) and then decreases (2–3%). This is consistent with the XRD results. The sample with $x = 2\%$ has the largest grain size and the most uniform grain size.

Fig. 4 exhibits the typical leakage current density behaviour (*J–E* curves) of BFNO films. From the diagram, we can clearly see that the symmetry of *J–E* curves in all BFNO films between negative and positive applied electric fields is good. In addition, the leakage current of all the samples increase as the examined electric field increase. We can clearly see that the leakage current of all Ni-doped BFO films is lower than the undoped one. Interestingly, with the increase of Ni-doped content from 0 to 2%, the leakage current of BFO film decreases. This behaviour was attributed to two following factors. On the one hand, with the increase of Ni^{2+} doping, the number of $(Ni^{2+}_{Fe^{3+}})'$ increases, which can be combined with the free movement ($(V_{O^{2-}})^{\cdot\cdot}$), while the formation of complex defects ($[(Ni^{2+}_{Fe^{3+}})' - (V_{O^{2-}})^{\cdot\cdot}]$ limit the

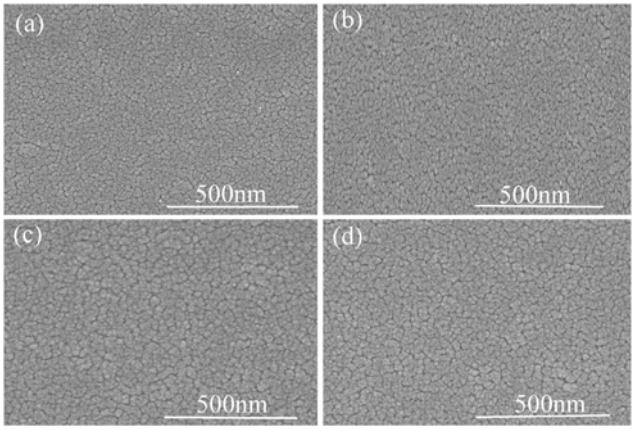

Fig. 3 *SEM surface morphology images of BFNO films*
a $x = 0$
b $x = 1\%$
c $x = 2\%$
d $x = 3\%$

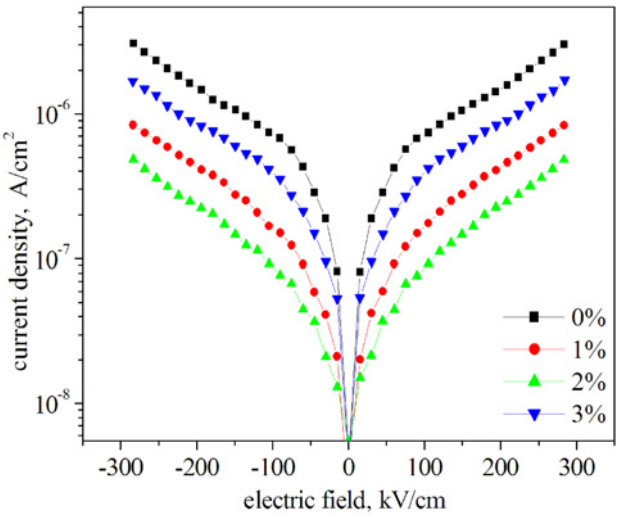

Fig. 4 *J–E curves of BFNO films in semilogarithmic*

movement of $(V_{O^{2-}})^{\cdot\cdot}$. On the other hand, the increased of $(Ni^{2+}_{Fe^{3+}})'$ can suppress the Fe^{3+} into Fe^{2+}. However, continue to increase the Ni^{2+} content to 3%, the leakage current density does not continue to decrease, but increase. Which attribute to that Ni^{2+} doping introduces more oxygen vacancies to make up for the unbalanced charge. The sample with $x = 2\%$ has the minimum leakage current density, which is 4.79×10^{-7} A/cm^2 at tested electric field of 300 kV/cm.

The leakage mechanism is important for understanding the source of leakage and reducing leakage. For the thin film material of the M-F-M capacitor structure we have built for test, conductance mainly comes from two parts: interface-limited processes and bulk-limited processes [24]. Ohmic conduction and space-charge-limited conduction (SCLC) are two of the most common types of bulk-limited processes. The leakage current mechanisms for BFNO films are analysed using a graph of log (J) and log (E), as shown in Fig. 5. The Ohmic conduction is a transmission mechanism that current and voltage show linear relationship. At low electric field, the electrons injected from the electrode are very few. The conductivity of the thin film is mainly generated by the free electrons located in the conduction band and the holes in the valence band. The relationship between the leakage current density (J) and the electric field intensity (E) follows Ohm's law [25]

$$J_{\text{ohmic}} = e\mu N_e E \tag{1}$$

where e, μ, N_e and E are electron charge, free carrier mobility, heat excited electron density and electric field intensity, respectively. In low electric field region, the α values are determined to be 1.10, 1.17, 1.08 and 1.10 for the for BFNO films with $x = 0$, 1, 2 and 3%, respectively. In other words, that leakage is given priority to with ohmic conduction ($\alpha \sim 1$) [26, 27]. The free electron density is caused by thermally stimulated electrons [28]. Next, let us talk about SCLC which is similar to electron conduction in vacuum diodes. The defects in the film, such as ion vacancies, interstitial atoms, can capture carriers and form a built-in electric field opposite to the direction of the applied electric field in the film, limited the movement of the charge to form a space charge limited current. The formula is as follows [29]:

$$J_{\text{SCLC}} = \frac{9\mu\varepsilon_r\varepsilon_0}{8d}E^2 \tag{2}$$

where μ, ε_r, ε_0, d and E are free carrier mobility, relative permittivity, vacuum dielectric constant, the film thickness and electric field intensity, respectively. The α is equal to 2 for SCLC. The α values are determined to be 2.01, 1.90, 2.01 and 1.91 at high tested electric

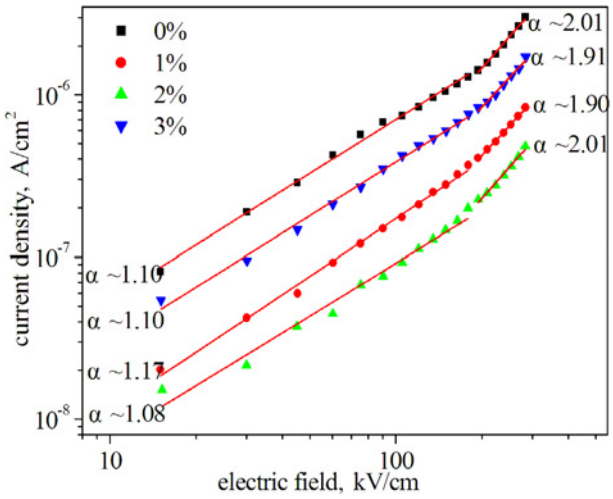

Fig. 5 *J–E curves of BFNO films in logarithmic plots*

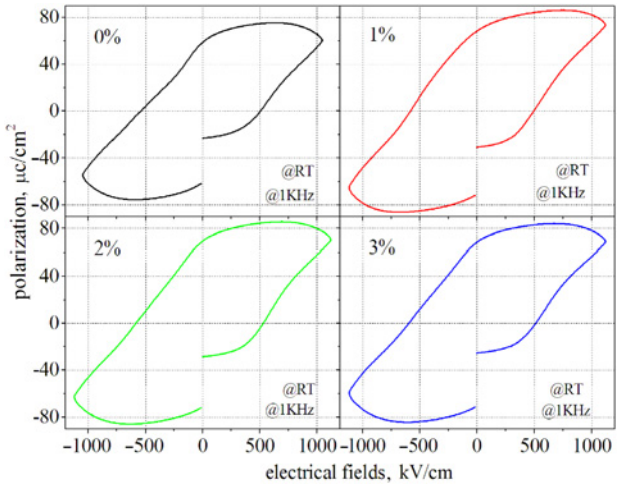

Fig. 6 *P–E hysteresis loops of BFNO films*

field for BFNO films with $x = 0$, 1, 2 and 3%, respectively. So, we can obtain that SCLC is dominant mechanism for all samples. In the high electric field area, the free electron density owing to carrier injection is bigger than the thermally excited electron density [30]. As a result, Ni doped does not cause significant change in the conduction mechanism.

Fig. 6 shows the polarisation-electric filed (P-E) hysteresis loops of BFNO films measured at RT and a 1 kHz frequency. In the application field of 1067 kV/cm, we obtained the saturation of the hysteresis loop. Perfected ferroelectric properties were obtained, for example large double remnant polarisation ($2P_r$), in comparison to the pure BFO film. The tested $2P_r$ and $2E_c$ values for the BFO film were 120.5 μC/cm^2 and 734 at 1067 kV/cm, respectively. The BFO film exhibits a poor loop due to a large contribution from the large current. With the increase of Ni-doped content from 1 to 3%, the remnant polarisation intensity increases first and then decreases. The sample with $x = 2\%$ has the maximum value of remnant polarisation ~141.4 μC/cm^2 at 1067 kV/cm. Base on the XRD result, the following factors can explain this behaviour. (i) a high diffraction peaks of (012) and (104)/(110), (ii) the largest grain size (large grain size leads to more easily flipped ferroelectric domains, thus improve the remnant polarisation).

4. Conclusion: A series of Ni-doped BFO films were prepared on the ITO/glass substrates by sol–gel method. We report the impact of Ni doped on the crystal microstructure, leakage current, conduction mechanism and ferroelectric behaviour systematically. From the XRD analysis, all samples match well with the perovskite structure without impurity phase. P-E hysteresis loop demonstrates that the optimal Ni-doped content of BFO films is $x = 2\%$, of which the remnant polarisation ($2P_r$) is 141.4 μC/cm^2 at electric field value of 1067 kV/cm. Leakage current density curves show that Ni doping has a great contribution in reducing leakage. The value of leakage is 4.79×10^{-7} A/cm^2 at tested electric field of 300 kV/cm. In addition, the leakage conduction mechanism transforms from the Ohmic conduction under the low electric field to the space charge limited conduction under high electric field. Ni doped does not cause significant change in the conduction mechanism.

5. Acknowledgments: This work was supported by funding from a Project of Shandong Province Higher Educational Science and Technology Program (grant no. J15LA05), Research Fund for the Doctoral Program of Shandong Jianzhu University (grant no. XNBS1626) and the National Natural Science Foundation of China (grant no. 51272142).

doi: 10.1049/mnl.2017.0554

6 References

[1] Catalan G., Scott J.F.: 'Physics and applications of bismuth ferrite', *Adv. Mater.*, 2009, **21**, (24), pp. 2463–2485

[2] Jia C.L., Urban K.W., Alexe M., *ET AL.*: 'Direct observation of continuous electric dipole rotation in flux-closure domains in ferroelectric $Pb(Zr,Ti)O_3$', *Science*, 2011, **331**, (6023), pp. 1420–1423

[3] Warusawithana M.P., Cen C., Sleasman C.R., *ET AL.*: 'A ferroelectric oxide made directly on silicon', *Science*, 2009, **324**, (5925), pp. 367–370

[4] Johann F., Morelli A., Vrejoiu I.: 'Epitaxial $BiFeO_3$ nanostructures fabricated by differential etching of $BiFeO_3$ films', *Appl. Phys. Lett.*, 2011, **99**, (8), pp. 2463–2465

[5] Ponzoni C., Rosa R., Cannio M., *ET AL.*: 'Optimization of BFO microwave-hydrothermal synthesis: influence of process parameters', *J. Alloy. Compd.*, 2013, **558**, (9), pp. 150–159

[6] Yan H.R., Deng H.M., Ding N.F., *ET AL.*: 'Influence of transition elements doping on structural, optical and magnetic properties of $BiFeO_3$ films fabricated by magnetron sputtering', *Mater. Lett.*, 2013, **111**, (45), pp. 123–125

[7] Xie J.J., Feng C.D., Pan X.H., *ET AL.*: 'Structure analysis and multiferroic properties of Zr^{4+} doped $BiFeO_3$ ceramics', *Ceram. Int.*, 2014, **40**, (1), pp. 703–706

[8] Cheng C.J., Borisevich A.Y., Kan D., *ET AL.*: 'Nanoscale structural and chemical properties of antipolar clusters in Sm-doped $BiFeO_3$ ferroelectric epitaxial thin films', *Chem. Mater.*, 2010, **22**, (8), PP. pp. 2588–2596

[9] Fan S., Xie X., Zhang F., *ET AL.*: 'Improved leakage and ferroelectric properties of Sr doped $BiFe_{0.95}Mn_{0.05}O_3$ thin films', *J. Mater. Sci.: Mater. Electron.*, 2016, **27**, (7), pp. 6854–6858

[10] Luo J.M., Lin S.P., Zheng Y., *ET AL.*: 'Nonpolar resistive switching in Mn-doped $BiFeO_3$ thin films by chemical solution deposition', *Appl. Phys. Lett.*, 2012, **101**, (6), pp. 2632–2636

[11] Huang F., Lu X., Lin W., *ET AL.*: 'Effect of Nd dopant on magnetic and electric properties of $BiFeO_3$ thin films prepared by metal organic deposition method', *Appl. Phys. Lett.*, 2006, **89**, (24), pp. 1719–1721

[12] Raghavan C.M., Kim J.W., Kim H.J., *ET AL.*: 'Preparation and properties of rare earth (Eu, Tb, Ho) and transition metal (Co) co-doped $BiFeO_3$ thin films', *J. Sol-Gel Sci. Technol.*, 2012, **64**, (1), pp. 178–183

[13] Wu J.G., Xiao D.Q., Wu W.J., *ET AL.*: 'Effect of dwell time during sintering on piezoelectric properties of $(Ba_{0.85}Ca_{0.15})(Ti_{0.90}Zr_{0.10})O_3$ lead-free ceramics', *J. Alloys Compd.*, 2011, **509**, (41), pp. L359–L361

[14] Rizvi M., Hakim M.A., Basith M.A., *ET AL.*: 'Size dependent magnetic and electrical properties of Ba-doped nanocrystalline $BiFeO_3$', *AIP Adv.*, 2016, **6**, (3), pp. 13–20

[15] Basu S., Hossain S.K.M., Chakravorty D., *ET AL.*: 'Enhanced magnetic properties in hydrothermally synthesized Mn-doped $BiFeO_3$ nanoparticles', *Curr. Appl. Phys.*, 2011, **11**, (4), pp. 976–980

[16] Hu Z.Q., Li M.Y., Yu Y., *ET AL.*: 'Effects of Nd and high-valence Mn co-doping on the electrical and magnetic properties of multiferroic $BiFeO_3$ ceramics', *Solid State Commun.*, 2010, **150**, (23), pp. 1088–1091

[17] Chauhan S., Kumar M., Chhoker S., *ET AL.*: 'Multiferroic, magnetoelectric and optical properties of Mn doped $BiFeO_3$ nanoparticles', *Solid State Commun.*, 2012, **152**, (6), pp. 525–529

[18] Yotburut B., Thongbai P., Yamwong T., *ET AL.*: 'Electrical and nonlinear current-voltage characteristics of La-doped $BiFeO_3$ ceramics', *Ceram. Int.*, 2017, **43**, (7), pp. 5616–5627

[19] Sen K., Thakur S., Singh K., *ET AL.*: 'Room-temperature magnetic studies of La-modified $BiFeO_3$ ceramic', *Mater. Lett.*, 2011, **65**, (12), pp. 1693–1965

[20] Fki H., Koubaa M., Sicard L., *ET AL.*: 'Influence of Y doping on structural, vibrational, optical and magnetic properties of $BiFeO_3$ ceramics prepared by mechanical activation', *Ceram. Int.*, 2017, **43**, (5), pp. 4139–4150

[21] Liu K.T., Li J., Wang L., *ET AL.*: 'Study on electric and magnetic properties of Ni-doped $BiFeO_3$ films', *J. Synth. Cryst.*, 2013, **42**, (9), pp. 1842–1847

[22] Kim J.W., Raghavan C.M., Choi J.Y., *ET AL.*: 'Effects of Ho- and Ni-doping alone and of co-doping on the structural and the electrical properties of $BiFeO_3$ thin films', *J. Korean Phys. Soc.*, 2015, **66**, (7), pp. 1051–1056

[23] Singh S.K., Maruyama K., Ishiwara H.: 'Reduced leakage current in La and Ni codoped $BiFeO_3$ thin films', *Appl. Phys. Lett.*, 2007, **91**, (11), pp. 112913–112913-3

[24] Huang A., Shannigrahi S.R.: 'Effect of bottom electrode and resistive layer on the dielectric and ferroelectric properties of sol-gel derived $BiFeO_3$ thin films', *J. Alloys Compd.*, 2011, **509**, (5), pp. 2054–2059

[25] Raghavan C.M., Kim E.S., Kim J.W., *ET AL.*: 'Structural and electrical properties of $(Bi_{0.9}Dy_{0.1})(Fe_{0.975}TM_{0.025})O_{3\pm\delta}$(TM = Ni^{2+}, Cr^{3+} and Ti^{4+}) thin films', *Ceram. Int.*, 2013, **39**, (4), pp. 6057–6062

[26] Qi X., Dho J., Tomov R., *ET AL.*: 'Greatly reduced leakage current and conduction mechanism in aliovalent-ion-doped $BiFeO_3$', *Appl. Phys. Lett.* 2005, **86**, (6), pp. 818–820

[27] Wu J., Wang J., Xiao D., *ET AL.*: 'Leakage mechanism of cation-modified $BiFeO_3$ thin film', *AIP Adv.*, 2011, **1**, (2), pp. 1218–1227

[28] Cho S.M., Jeon D.Y.: 'Effect of annealing conditions on the leakage current characteristics of ferroelectric PZT thin films grown by sol–gel process', *Thin Solid Films*, 1999, **338**, (1-2), pp. 149–154

[29] Wu J.G., Wang J., Xiao D.Q., *ET AL.*: 'Ferroelectric behavior in bismuth ferrite thin films of different thickness', *ACS Appl. Mater. Interfaces*, 2011, **3**, (9), pp. 3261–3263

[30] Raghavan C.M., Kim J.W., Kim S.S.: 'Effects of (Dy, Zn) co-doping on structural and electrical properties of $BiFeO_3$ thin films', *Ceram. Int.*, 2014, **40**, (1), pp. 2281–2286